RESEARCH ARTICLE

Human Mutation

OFFICIAL JOURNAL HGVS HUMAN GENOME VARIATION SOCIETY www.hgvs.org

Functional and Structural Analysis of Five Mutations Identified in Methylmalonic Aciduria *cblB* Type

Ana Jorge-Finnigan,[1] Cristina Aguado,[1] Rocio Sánchez-Alcudia,[1] David Abia,[2] Eva Richard,[1] Begoña Merinero,[1] Alejandra Gámez,[1] Ruma Banerjee,[3] Lourdes R. Desviat,[1] Magdalena Ugarte,[1]* and Belen Pérez[1]

[1]*Centro de Diagnéstico de Enfermedades Moleculares, Centro de Biología Molecular-SO UAM-CSIC, Universidad Autónoma de Madrid, Campus de Cantoblanco, Madrid, Spain/Centro de Investigación Biomédica en Red de Enfermedades Raras (CIBERER), ISCIII, Madrid, Spain;* [2]*Servicio de Bioinformática, Centro de Biología Molecular-SO UAM-CSIC, Madrid, Spain;* [3]*Department of Biological Chemistry, University of Michigan Medical Center, Ann Arbor, Michigan*

Communicated by David S. Rosenblatt

Received 11 November 2009; accepted revised manuscript 1 June 2010.
Published online 15 June 2010 in Wiley Online Library (wileyonlinelibrary.com). DOI 10.1002/humu.21307

ABSTRACT: ATP:cob(I)alamin adenosyltransferase (ATR, E.C.2.5.1.17) converts reduced cob(I)alamin to the adenosylcobalamin cofactor. Mutations in the *MMAB* gene encoding ATR are responsible for the *cblB* type methylmalonic aciduria. Here we report the functional analysis of five *cblB* mutations to determine the underlying molecular basis of the dysfunction. The transcriptional profile along with minigenes analysis revealed that c.584G>A, c.349-1G>C, and c.290G>A affect the splicing process. Wild-type ATR and the p.I96T (c.287T>C) and p.R191W (c.571C>T) mutant proteins were expressed in a prokaryote and a eukaryotic expression systems. The p.I96T protein was enzymatically active with a K_M for ATP and K_D for cob(I)alamin similar to wild-type enzyme, but exhibited a 40% reduction in specific activity. Both p.I96T and p.R191W mutant proteins are less stable than the wild-type protein, with increased stability when expressed under permissive folding conditions. Analysis of the oligomeric state of both mutants showed a structural defect for p.I96T and also a significant impact on the amount of recovered mutant protein that was more pronounced for p.R191W that, along with the structural analysis, suggest they might be misfolded. These results could serve as a basis for the implementation of pharmacological therapies aimed at increasing the residual activity of this type of mutations.
Hum Mutat 31:1033–1042, 2010. © 2010 Wiley-Liss, Inc.

KEY WORDS: methylmalonic aciduria cblB type; ATR; MMAB; misfolding; splicing; cobalamin

Introduction

ATP:cob(I)alamin adenosyltransferase (ATR, E.C.2.5.1.17) is an enzyme involved in vitamin B_{12} metabolism that converts reduced cob(I)alamin to adenosylcobalamin, the active cofactor of methylmalonyl-CoA mutase (MUT, EC 5.4.99.2), which catalyzes the reversible rearrangement of methylmalonyl-CoA to succinyl-CoA in the catabolism of branched-chain amino acids, odd-chain fatty acids, and cholesterol. Mutations in the human *MMAB* gene encoding the ATR enzyme are responsible for the *cblB* type methylmalonic aciduria (MIM# 607568) [Dobson et al., 2002; Leal et al., 2003]. *CblB* patients present either a severe form with neonatal ketoacidosis, lethargy, failure to thrive, and encephalopathy or a milder, chronic form with less impaired neurological outcome. A cellular in vitro response to hydroxocobalamin (OHCbl) has been reported in certain cases, but this response appears to be unclear in vivo.

The human *MMAB* gene product, the ATR enzyme, is a member of the PduO family of cobalamin adenosyltransferases, which catalyzes the transfer of adenosine from ATP to cobalamin generating AdoCbl. To date, 24 mutations have been identified in the *MMAB* gene in *cblB*-type patients (HGMD® Professional Release 2009.3). Recently, the crystal structures of the homologous ATR proteins from *T. acidophilum* and *L. reuteri*, along with the human enzyme with ATP bound, have been determined [Saridakis et al., 2004; Schubert and Hill, 2006; St. Maurice et al., 2007], allowing for evaluation of the structural impact of pathogenic mutations in ATR. The enzyme is a homotrimer, each subunit composed of a five-helix bundle and an active site located at the subunit interface. Several mutations identified in patients have been mimicked in prokaryotic orthologs and their kinetic parameters determined. They revealed the existence of mutants with reduced affinity for the substrate and cofactor (p.R191W) and with negligible activity and presumed instability in vivo (p.R186W, p.R190H, and p.E193K) [Zhang et al., 2006]. In another study, a *Salmonella* ATR-deficient strain was used to express mutations generated by random mutagenesis in the human ATR coding sequence, allowing the delineation of the active site of the enzyme and the putative residues implicated in cob(II)alamin reduction [Fan and Bobik, 2008].

In this study, we report the genetic analysis of four methylmalonic aciduria *cblB*-type patients and the functional analysis of the identified mutations. In order to determine the molecular basis of in vitro B_{12} responsiveness we have functionally analyzed two missense changes, p.I96T and p.R191W, identified in three B_{12} responsive patient-derived cell lines, in prokaryotic and eukaryotic in vitro expression systems. We have also included the functional analysis of the three mutations affecting splicing (c.290G>A, c.584G>A, and c.349−1G>C) in an ex vivo assay using minigenes.

Cristina Aguado's present address is Universidad Pompeu Fabra.

*Correspondence to: Magdalena Ugarte, Centro de Biología Molecular "Severo Ochoa" CSIC-UAM, C/Nicolás Cabrera No. 1, Universidad Autónoma de Madrid, 28049 Madrid, Spain. E-mail: mugarte@cbm.uam.es

Materials and Methods

Genetic and Biochemical Analysis in Patients' Fibroblasts

Patient 1 (P1), previously described in Merinero et al. [2008], had a neonatal presentation of the disease. Patients 2 (P2) and 3 (P3) are siblings; P2 developed a late onset of the disease (at 4 years) and died shortly afterward. P3 was genetically diagnosed without presenting clinical symptoms, and to date, he is clinically normal. Patient 4 (P4) was referred to our laboratory for genetic analysis (Table 1). Since diagnosis, both the asymptomatic patients P3 and P4 are under therapy with protein restriction, carnitine supplementation, OHCbl administration, oral (5 ml/d) in P3, and intramuscular (5 mg/15 days) in P4 and metronidazol (only P4). During therapy the patients show differences at the biochemical level: P3 shows milder plasma C3 levels (~10 μM) compared to P4 (80 μM); P3 has normal plasma odd-chain fatty acid levels (OLCFA) (<0.4%), whereas P4 has increased ones (~4%). Urine MMA varies in P3 (<200–6000 mmol/mol creat), whereas there are no data available from P4. P3 has a perfect clinical development according to the clinician. P4 has a normal neurological and cardiological evaluation with normal renal function, weight (percentile 25–50) and height (percentile 10) and he is doing well at school. Due to reduction of bone density in lumbar spine, alandronate, calcium, and vitamin D were administered within growth and bone density. During his life he has showed some other metabolic decompensations associated with infections, vomiting, metabolic ketoacidosis, etc., without requiring hospital admission. In these crises the patient required nutritional adaptation. It is worth noting that the patient has excellent dietary compliance. This work has been approved by our institutional ethics committee, and informed consent has been obtained from the patients and their legal caregivers.

Fibroblast cell lines from patients were cultured under standard conditions in MEM supplemented with 10% fetal bovine serum, 200 mM glutamine, and antibiotics. Incorporation of radioactivity from [1-^{14}C] propionate into acid-precipitable material was assayed in intact fibroblasts grown in basal medium ±1 μg/ml OHCbl as previously described [Perez-Cerda et al., 1989]. All data are summarized in Table 1.

To identify mutations in the *MMAB* gene, cDNA sequence analysis was performed. The identified changes were confirmed by sequencing the corresponding genomic DNA region. Genotype analysis was performed using the primers and conditions described previously [Martinez et al., 2005]. Fibroblast cell lines were used as a source of DNA and RNA, which were isolated using the MagnaPure system following the manufacturer's protocol (Roche Applied Sciences, Indianapolis, IN). Mutation nomenclature follows the recommended guidelines of the Human Genome Variation Society (www.HGVS.org). Nucleotide numbering is based on cDNA reference sequences GenBank accession number NM_052845.3.

Functional Analysis of the Splicing Mutations

For evaluation of in vitro splicing, the pSPL3 vector (Life Technologies, Gibco, BRL, Grant Island, NY, kindly provided by Dr. B. Andresen, Aarhus University, Denmark) was used. Gene fragments corresponding to exons and flanking intronic regions were amplified from patients P2 and P4 and from a DNA control and cloned into the TOPO vector (Invitrogen, Carlsbad, CA) as previously described [Rincon et al., 2007]. A total of 2 μg of the wild-type or mutant minigenes was transfected into the following cell lines: Hep3B, HEK293, or COS7 using JetPEI, following the manufacturer's recommendations. Twenty-four to 48 hr postransfection, cells were harvested, RNA was purified, and RT-PCR analysis was performed using the pSPL3-specific primers SD6 and SA2 (Exon Trapping System, Gibco, BRL). The identity of amplified bands was determined by sequence analysis.

Prokaryotic and Eukaryotic Expression Analysis of Missense Changes

Mutation p.I96T (c.287T>C) and p.R191W (c.571C>T) were introduced using the QuikChange Site Directed Mutagenesis kit (Stratagene, Cedar Drive, TX). The oligonucleotides used for mutagenesis were: *MMAB* I96Tsense (5′AGTTCAGCTACTGGGTTTGCTCTG3′), *MMAB* I96T antisense (5′CAGAGCAAACCCAGTAGCTGAACT3′), *MMAB*R191W sense (5′CCGTGTGCCGCTGGGCCGAGAGAC3′) and *MMAB* R191W antisense (5′GTCTCTCGGCCCAGCGGCACACGG3′).

For prokaryotic expression analysis we used the NL173 plasmid, based on pET41a, which contains the human ATR sequence without the mitochondrial targeting sequence. Human ATR protein was expressed in *Escherichia coli* (BL21Star^{TM}DE3 One Shot Cells) and purified following the method described by Leal et al. [2004]. Bacterial cells were transformed with the NL173 plasmid encoding either the normal or mutant (p.I96T and p.R191W) ATRs. Protein expression was induced with 1 mM IPTG; 5 hr after induction, cells were collected by centrifugation and frozen at −70°C until further use. Cell pellets were resuspended at 4°C in 50 mM potassium phosphate buffer, pH 8, 100 mM NaCl, 1 mM DTT, 1 mM protease inhibitor phenylmethylsulphonyl fluoride, 1 mM EDTA, 0.05 mg/ml DNase, 0.3 mg/ml lysozyme. After 1 hr of incubation, the cell suspension

Table 1. Genotype, Clinical and Biochemical Phenotype in Four Methylmalonic Aciduria Patients *cblB* Type

Patient	MUT activity[b] (nmol/min/mg)	[1-^{14}C]-propionate −/+[c]	Allele 1	Allele 2	Onset	Outcome
P1	0.99	0.06/0.25	p.I96T (c.287T>C)	p.R191W (c.571C>T)	Neonatal (4 days)	7 y/severe encephalopathy
P2[a]	0.76	0.26/1.01	p.I96T (c.287T>C)	p.S174fs (c.584G>A)	Late onset (4 years)	Died at 4 y
P3[a]	NS	NS	p.I96T (c.287T>C)	p.S174fs (c.584G>A)	studied due to previous affected sister (3 months)	5 y/asymptomatic
P4	0.55	0.08/0.07	p.I117_Q118del (c.349−1G>C)	p.G66fs (c.290G>A)	Neonatal (4 days)	12 y/asymptomatic

NS, not studied. Mutation nomenclature follows the recommendations of HGVS and cDNA numbering is based on GenBank accession number NM_052845.3.
[a]Patients 2 (P2) and 3 (P3) are siblings.
[b]MUT activity in control fibroblasts with 36 μM AdoCbl was 0.94±0.40 nmol/min/mg protein.
[c][1-^{14}C]-Propionate uptake (nmol/10 hr/mg protein) in control fibroblasts without/with (−/+) hydroxocobalamin in the culture medium was 1.90±1.18/2.34±1.61.

was sonicated and centrifuged to obtain the crude soluble cell extract, which was subjected to ammonium sulphate precipitation and subsequent anion-exchange chromatography using a Sepharose Q column, as previously described [Leal et al., 2004]. In all purification steps, protein concentration was determined by the Bradford assay. Fractions eluted from the Sepharose Q column were subjected to SDS-PAGE to identify those enriched with the ATR protein. In some cases before ATR enzymatic assay, wild-type and mutant ATR proteins were further purified by hydroxyapatite chromatography at 4°C using as mobile phase a gradient of 10–400 mM potassium phosphate buffer pH 8, and 5 mM KCl. Fractions containing ATR of the highest purity were pooled and concentrated using an Amicon concentrator to a final concentration of 10 mg/ml.

Full-length cDNA of wild-type *MMAB* was generated from total RNA fibroblasts by RT-PCR and cloned into pGEM-T vector (Promega, Madison, WI). Subsequently, *MMAB* cDNA was further excised and inserted into *Hind*III/*Eco*RV sites of pFLAG–CMV-5c expression vector (Sigma, St. Louis, MO) to obtain *MMAB* cDNA coupled with FLAG-tag at the C-terminus (pFLAG–*MMAB*).

Eukaryotic expression analysis was performed in the P4 fibroblast cell line stably transformed with pBABE kindly provided by Dr. JA Enriquez (University of Zaragoza, Spain). A total of 4×10^5 transformed cells were transfected using 2.5 μg of normal or mutant pFLAG–*MMAB* constructs using lipofectamine 2000 (Invitrogen); then the cells were grown at 27 or 37°C. Harvested cells were used to determine ATR activity, which was indirectly measured by the analysis of [^{14}C]-propionate incorporation into acid-precipitable material in intact cells grown in basal medium [Perez-Cerda et al., 1989]. Propionate oxidation is catalyzed by two mitochondrial enzymes: the biotin-dependent propionyl-CoA carboxylase and the AdoCbl-dependent methylmalonyl-CoA mutase. AdoCbl is synthesized by ATR, and the patients with defects in the *MMAB* gene exhibit deficient propionate incorporation. Statistical analysis was performed using an *F*-test analysis of variance followed by a one-tailed paired *t*-test. Values of $P < 0.05$ were considered significant.

Enzyme Activity Assays

ATR activity was measured as previously published [Johnson et al., 2001] with minor modifications. Assays contained 200 mM Tris-HCl pH 8.0, 1.6 mM KH_2PO4, 2.8 mM $MgCl_2$, 100 mM KCl, 0.4 mM ATP, and 80 μM OHCbl (Sigma-Aldrich, St. Louis, MO). A total of 800 μl aliquots of the reaction mixture was dispensed into cuvettes kept at 37°C. Titanium (III) citrate (10 μl) was added, the reaction initiated by the addition of 10–100 μg of purified protein, and the decrease in absorbance at 388 nm was monitored. Anaerobic procedures were used to prepare the reaction mix, the protein solution and titanium(III)citrate.

Measurement of Dissociation Constants

The equilibrium dissociation constants (K_d) for cob(II)alamin analogs were determined fluorimetrically as described by Chowdhury and Banerjee [1999] with modifications. To determine the K_d values, 40–150 μg of protein in 50 mM Tris-HCl buffer, pH 8.0, were added to a quartz cuvette and successive aliquots (1–10 μl) of the cobalamin analogue (2–7 mM) were added, then the fluorescence (excitation wavelength: 280 nm, emission wavelength 340 nm) was measured after each addition. The K_d for cob(II)alamin was determined under anaerobic conditions by monitoring the shift in the UV-visible spectrum from 300 to 750 nm using 10 μM cob(II)alamin and varying concentrations of ATR as described previously [Yamanishi et al., 2005]. The kinetic data were analyzed using the IGOR Pro6 software (WaveMetrics Inc, Lake Oswego, OR).

Western Blot Analysis

Protein concentration in fibroblast and bacterial cell extracts was determined using the BIO-RAD protein assay (Bio-Rad, Bio-Rad Laboratories, Munchen, Germany) following the manufacturer's protocol. Equal amounts of total protein for bacterial cell extracts were loaded onto a 10% Laemmli SDS-PAGE System. After SDS-PAGE or native gel electrophoresis, proteins were transferred to a nitrocellulose transfer membrane (GE Healthcare, Buckinghamshire, UK) using a BIO-RAD apparatus in Tris (25 mM)–glycine (192 mM)–methanol (20%) without SDS for 1 hr. Poinceau staining was used to monitor equal loading of protein. Immunodetection was carried out using commercially available anti-ATR antibodies (ProteinTech Group Inc, Chicago, IL) as primary antibodies diluted 1:1,000. The secondary antibodies used were conjugated goat–antimouse IgG-horseradish peroxidase (1:10,000) (Santa Cruz Biotechnology Inc, Santa Cruz, CA) and were detected using the Enhanced Chemiluminescence System (GE Healthcare). Relative protein amounts were determined using a calibrated densitometer GS-800 (BioRad, Hercules, CA).

Oligomeric State of ATR

Size-exclusion chromatography using a Superdex 200 (1.2×92 cm) column was performed to assess the oligomeric state of the wild-type and mutant ATR proteins. A total of 100 μg of protein purified by ammonium sulphate precipitation and anion-exchange chromatography was applied to the column in 50 mM Tris-HCl buffer pH 8.0, 100 mM KCl, and a flow rate of 2.0 ml min^{-1}. Molecular mass value estimations were obtained using a calibration curve generated with molecular weight standards (BioRad).

Blue native electrophoresis was performed using 4–16% Native PAGE gels, Native Marker, and Native running buffer from Invitrogen. Samples were prepared with 4 × Native sample buffer with G-250 sample additive (Invitrogen). The electrophoretic separation was performed at 4°C for 1 hr at 150 V, followed by another hour at 250 V. Lanes containing purified ATR and molecular weight marker were stained using 2% Coomassie Brilliant Blue R-250 (BioRad) solution in acetic acid and destained in acetic acid: methanol: water (0.5:2:2). The remaining lanes were transferred to a PVDF membrane using the iBLOT system from Invitrogen. Immunodetection was carried out as described above.

Protein Stability Studies

The stability of the wild-type and mutant p.I96T and p.R191W proteins expressed in the prokaryotic system was investigated by incubating the transformed cells at 37 or 27°C following IPTG induction. Soluble supernatant was incubated at 37 or 27°C, aliquots were removed at different time points, and the cell extracts were subjected to SDS-PAGE. Western blot analysis was performed as described above. Following densitometric analysis, relative protein levels were expressed as percentage referred to time 0.

Structural Analysis and Molecular Dynamics

Visualization of the crystal structure of ATR and localization of the mutant residue I96 was performed using DSViewerPro5.0 (Accelrys Inc, San Diego, CA) with the PDB coordinates file 2IDX.

Human ATP:cobalamin adenosyltransferase (hATR) monomers were modeled using as a template the B and C chains from the PDB structure 2IDX [Schubert and Hill, 2006], and the program MODELLER9v7 [Eswar et al., 2006]. The ATP binding loop "KIYTK" was kept in the bound conformation from chain B, while the unresolved loop "SSAREAHLKYT" in the B chain was taken from the C chain. Trimer reconstruction was performed by superposition of the modeled monomer over the 2IDX structure with the help of the MAMMOTH program [Ortiz et al., 2002]. All three active sites were modeled as occupied by an ATP molecule.

Models of mutants p.R191W and p.I96T were generated with the program PyMOL [DeLano, 1998–2003] using the modeled trimer as template. Protonation states of ionizable groups at pH 6.5 for the three systems were calculated using the H++ server [Gordon et al., 2005]. The positions of hydrogen atoms, standard atomic charges, and radii for all the atoms were assigned according to the ff03 force field [Duan et al., 2003]. The complexes were immersed in cubic boxes of TIP3P water molecules [William et al., 1983] large enough to guarantee that the shortest distance between the solute and the edge of the box was larger than 13 Å. Counterions were also added to maintain electroneutrality. Three consecutive minimizations were performed involving: (1) only hydrogen atoms, (2) only the water molecules and ions, and (3) the entire system.

Simulation Details

Starting minimized structures, prepared as stated above, were simulated in the NPT ensemble using Periodic Boundary Conditions and Particle Mesh Ewald to treat long-range electrostatic interactions. The systems were then heated and equilibrated in two steps: (1) 200 ps of molecular dynamics (MD) heating the whole system from 100 to 300 K, and (2) equilibration of the entire system during 1.0 ns at 300 K. The equilibrated structures were the starting points for the 15 ns MD simulations at constant temperature (300 K) and pressure (1 atm). SHAKE algorithm was used to keep bonds involving H atoms at their equilibrium length, allowing a 2-fs time step for the integration of Newton's equations of motion. ff03 and TIP3P force fields, as implemented in AMBER 10 package [Case et al., 2008], were used to describe the proteins, the peptides, and the water molecules, respectively. Sample frames at 10-ps intervals from the molecular dynamics trajectory were subsequently used for the analysis.

In Silico Stability Analysis

Absolute free energies of the hATR complex and its mutants (p.R191W and p.I96T) were estimated using the MM-GBSA [Still et al., 2002] approach as implemented in the AMBER10 package. MM-GBSA method approaches the free energy of the complexes as a sum of a molecular mechanic (MM) interaction term, a solvation contribution through a generalized Born (GB) model, and a surface area (SA) contribution to account for the nonpolar part of solvation. Distributions of the observed free energies, measured every 10 ps snapshots along with the molecular dynamics simulations, were plotted using the R package [Gentleman, 1997].

In addition, to better characterize the changes produced by the mutated residues, an energy decomposition analysis in a pairwise fashion (between the residues surrounding the mutations) was performed using a cutoff of 5 Å from the mutated residues. Polar contribution to solvation free energies were calculated with GB, whereas nonpolar contributions were estimated to be proportional to the area lost upon binding using the LCPO method to calculate accessible surface areas [Weiser et al., 1999].

These calculations were performed, for each 10-ps snapshot from the simulations, using the appropriate module within AMBER 10 package. Free-energy decomposition interaction matrix was represented in an energy dependent color gradient using the program matrix2png [Pavlidis and Noble, 2003].

Results

P1, P2, and P4 patients showed normal MUT activity and P1 and P2 exhibited in vitro responsiveness to B_{12} (Table 1). The age of onset and the clinical outcome of these patients are summarized in Table 1. The p.I96T (c.287T>C) sequence change was identified in three of the patients (P1, P2, and P3). This mutation was found in combination with the missense change p.R191W (c.571C>T) and in two siblings in combination with c.584G>A mutation, affecting the last nucleotide of exon 7 in the *MMAB* gene. This last mutation results in exon 7 skipping (r.520_584del) in patient fibroblasts, which would result in a premature stop codon (p.S174fs) (Fig. 1A).

The RT-PCR pattern and subsequent sequence analysis of the amplified products obtained from patient P4 fibroblasts, showed the presence of two bands, one of them corresponding to the skipping of exon 3 (r.197_290del), which is predicted to generate a truncated protein and the other one corresponding to an in-frame deletion of two amino acids (r.349_354del6, p.I117_Q118del) due to activation of a cryptic splice site inside exon 5. The genomic DNA analysis showed two nucleotide changes c.290G>A and c.349−1G>C in the last nucleotide of exon 3 and in the 3′ splice site of intron 4, respectively (Fig. 1B).

Functional Analysis of the Splicing Mutations

In this work, we have investigated the functional effect of the three nucleotide changes affecting splicing (c.290G>A, c.349−1G>C, and c.584G>A) using a cell-based splicing assay. In the patient fibroblasts, only transcripts resulting from the skipping of exon 7 and exon 3 derived from the c.584G>A and c.290G>A alleles are detected. However, if correct splicing occurred occasionally, a mutant protein with the p.R195H and p.G97E changes would result. A minigene functional splicing assay was employed to investigate this possibility. All splicing mutations were cloned in minigenes and transfected in Hep3B, HEK293, or COS cells. All the mutants resulted in aberrant splicing. In addition of the strong 3′ and 5′ splice sites, the pSPL3 vector has after the multiple cloning site, cryptic 3′ and 5′ splice sites. In the case of the c.290G>A and c.584G>A mutant constructs, both splicing sequences were used—the classical and the cryptic one—and therefore the fragment amplified contained a vector sequence generated from use of the weaker cryptic spice sites (Fig. 2) In the case of c.584G>A a small but detectable amount of the correctly spliced transcript (resulting in the p.R195H change) was observed.

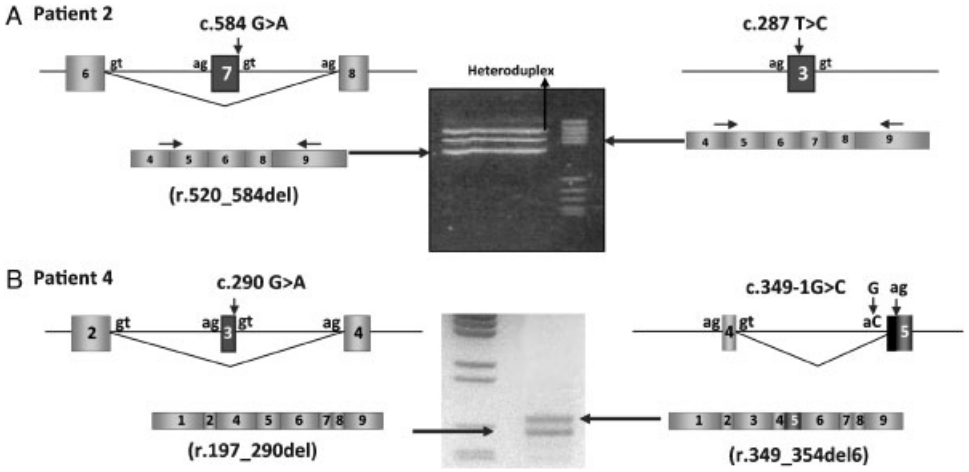

Figure 1. Schematic representation of the mutations mapped in genomic DNA and RT-PCR pattern from fibroblast. **A:** Patient P2 carries one nucleotide change located on exon 7 (c.584G > A) and a missense change on exon 3 (c.287C > T; p.I96T). The transcriptional profile shows three bands corresponding to the skipping of exon 7 transcribed from the allele bearing the c.584G > A change, a normal band from the allele bearing the c.287 T > C and a heteroduplex extra band (upper band). **B:** Patient 4 carries a change located on the last nucleotide of exon 3 (c.290 G > A) and an intronic change (c.349−1G > C) in intron 4. The RT-PCR pattern shows a smaller band without exon 3 resulting from the c.290G > A change and a larger one with an in-frame deletion of the first six nucleotides of exon 5 from the allele bearing c.349−1G > C.

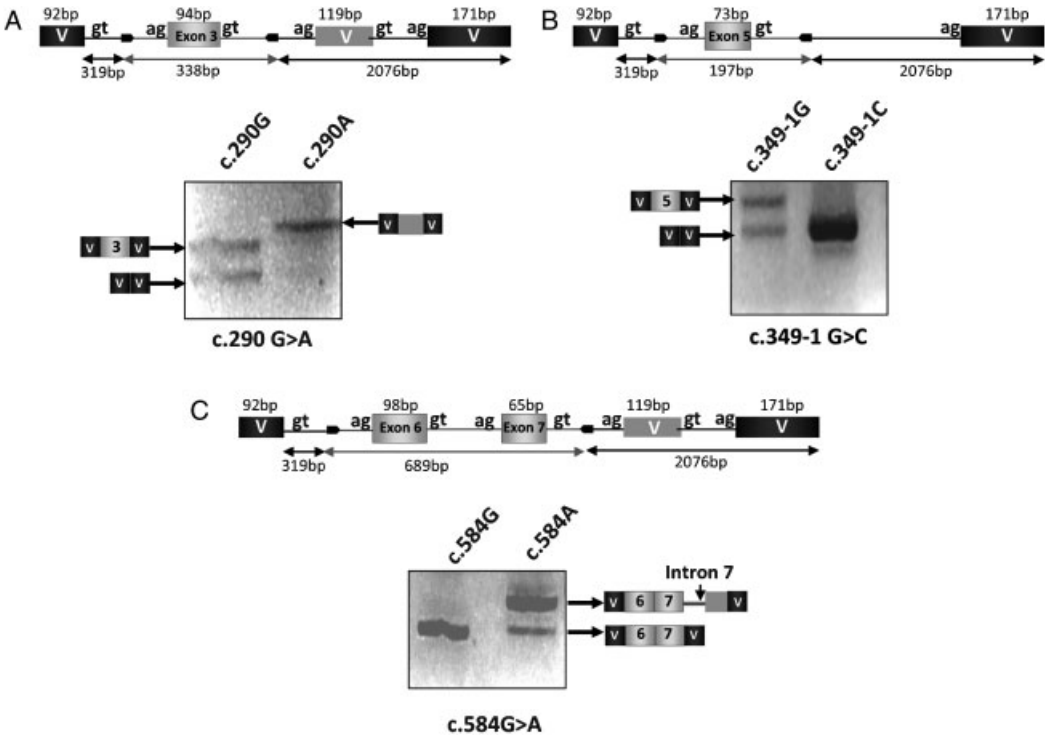

Figure 2. Splicing cellular minigene analysis. RT-PCR pattern obtained after transfection with the corresponding wild-type and mutant minigene constructs and schematic representation of each minigene construct. The PCR from the c.290G > A and c.349−1G > A minigenes was performed using minigene-specific primers while in the c.584G > A, a specific forward primer located at the junction of the vector sequence, and exon 6 was used to prevent different bands obtained when minigene-specific primers are used. All fragments were sequenced and the schematic representation of the resultant transcripts is indicated. Gene fragments corresponding to exon 3 (**A**) or exon 5 (**B**) and flanking 3′ and 5′ intronic regions were amplified from patients and cloned into the pSPL3 vector (gray line and box). For the c.584G > A minigene, the amplified fragment included exon 6, intron 6, and exon 7 and also the intronic sequence adjacent to both exons. The exonic sequences of the pSPL3 vector are highlighted in black boxes (V-boxes: vector sequence) and shaded boxes refers to the sequences involved when the cryptic splice sites are used (**A** and **C**). The sequence of the RT-PCR fragment obtained with the normal minigene (c.290G, c.349−1G, and c.584G) revealed the presence of a normal transcript with the corresponding exon included. In the two former cases we have also detected a slight band corresponding to a complete skipping of exon 3 and 5 that cannot be amplified in the third case. The sequence of the fragment obtained after transfection with the mutant construction containing the c.290A or c.584A changes revealed the presence of a vector sequence of 119 bp inserted in the aberrant transcript due to activation of a 3′ and 5′ cryptic splice site located in the vector sequence following the poly-cloning site.

Functional and Structural Analysis of the Missense Mutations

Because the three patients responsive to B_{12} in vitro share the p.I96T mutation described previously [Merinero et al., 2008], we sought to analyze the kinetic stability properties of the mutant protein. Residue I96 is located in helix α1 (Fig. 3A), distant from the ATP binding site, whereas residue R191 projects into the central cavity of the trimeric protein. Given the location of the I96 residue in α1 helix, the mutation could change the stability of the protein and/or perturb binding of the substrates, ATP, and cobalamin, but is not predicted to be involved in trimer formation.

Absolute free energies for wild-type hATR and the mutants, p.R191W and p.I96T, were estimated by the MM-GBSA method and predicted a decrease in stability for the p.R191W mutant ($-15{,}026.93 \pm 68.35$ kcal/mol) compared to the wild-type ATR (-15436.88 ± 72.76 kcal/mol) or the p.I96T mutant ($-15{,}441.07 \pm 67.06$ kcal/mol). In fact, a significant difference was not found between wild-type ATR and the p.I96T mutant (Supp. Fig. S1).

In addition, pair-wise interaction energies were calculated for the residues surrounding the mutations. In p.R191W, a network of hydrogen bonds at the trimer centre involving R191 and E91 residues was detected, linking the three monomers (Fig. 3B). The equivalent interaction in p.R191W mutant is substantially diminished (Fig. 3C). However, this energy loss is compensated,

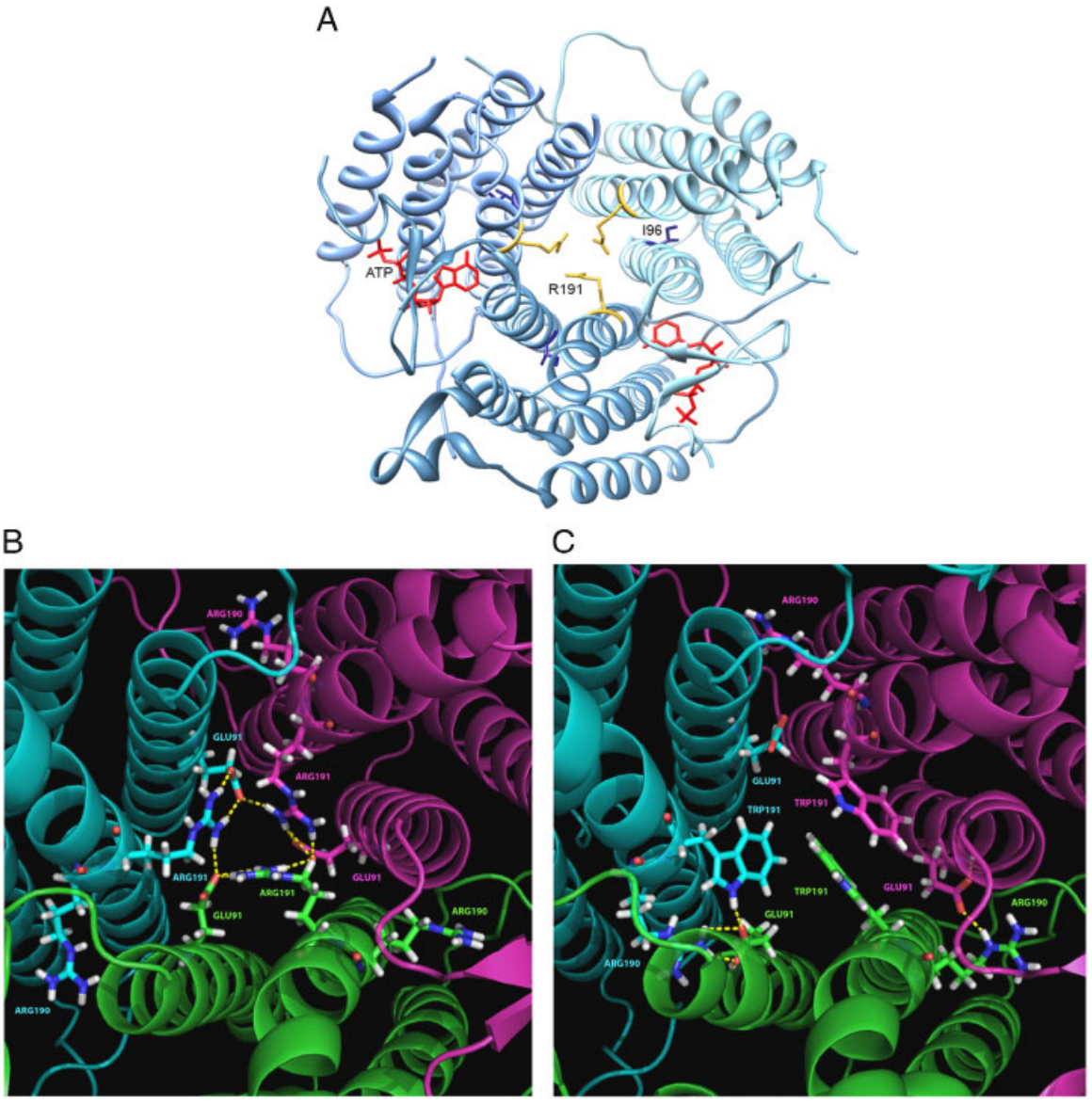

Figure 3. Structural analysis of missense mutation. **A:** Location of the p.I96T and p.R191W mutations in the crystal structure of human ATR. The enzyme is a homotrimer, with each subunit (shown in a different shade of blue) composed of a five-helix bundle and with the active site located at the subunit interfaces. Residue I96 is located in helix α1, distant from the ATP binding site, while residue R191 projects into the central cavity of the trimeric protein. ATP (red) and the residues, I96 (blue) and R191 (gold) are shown in stick representation. This figure was generated from the PDB file 2idx. **B:** Wild-type hATR trimer core (represented as cartoon) showing hydrogen bonds (dashed yellow lines) between residues E91, R190, and R191 (represented as sticks). **C:** R191W mutant hATR trimer core (represented as cartoons) showing hydrogen bonds (dashed yellow lines) between residues E91, R190, and R191 (represented as sticks).

Table 2. Comparison of Kinetic Parameters for Wild-Type and p.I96T ATR

	Wild type	p.I96T
Specific activity (nmol min^{-1} mg^{-1})	200 ± 10	123 ± 19
K_M (μM) ATP	6.2 ± 1.3	7.8 ± 1.9
K_d (μM) AdoCbl	1.7 ± 0.4	2.58 ± 0.62
K_d (μM) OHCbl	8.5 ± 1.1	7.8 ± 1.6
K_d (μM) CNCbl	7.8 ± 0.5	13.3 ± 0.3
K_d (μM) Cob(II)alamin	3.6 ± 1.6	1.37 ± 0.33

Data are the mean of at least two independent experiments each performed in duplicate.

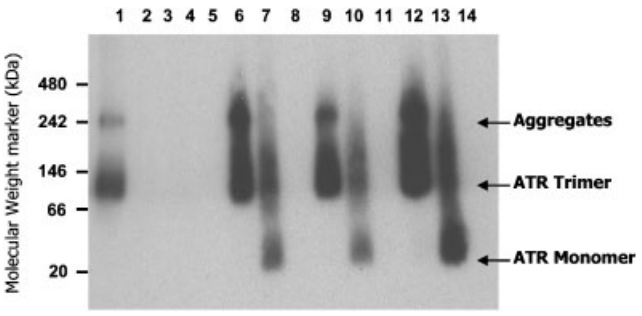

Figure 4. Oligomeric state of ATR. Blue native gel electrophoresis of cell extracts subjected to immunodetection for ATR. Lane 1, 1 μg of purified wild-type hATR; lane 2, total extract from nontransformed BL21 bacteria; lanes 3–5, whole-cell extracts from uninduced bacteria transformed with wild-type ATR plasmid (lane 3), p.I96T ATR (lane 4), and p.R191W ATR (lane 5); lanes 6–14 induced transformed bacteria. Lanes 6, 7, and 8, whole-cell extracts of wild-type (1 μg), p.I96T (2.5 μg), or p.R191W (20 μg); lanes 9, 10, and 11, supernatant of wild-type (1 μg), p.I96T (2.5 μg), and p.R191W (20 μg) after centrifugation of sonicated cell extracts; lanes 12, 13, and 14, pellets from wild-type (1 μg), p.I96T (2.5 μg), and p.R191W (20 μg) obtained after centrifugation.

at least in part, by a new inter subunit hydrogen bond pattern established between the R190 and E91 residues. In addition, the effect of the stacked conformation adopted by the mutant W191 residue creates a distortion in the trimer core that is reflected by other changes involving the interaction profile of E84, especially those related to R194 and R195, and the interaction between R190 and bound ATP (data not shown). On the contrary, a significant difference in the pair-wise interaction energy when comparing the I96T mutant to the wild-type protein was not observed.

Wild-type and mutant (p.I96T) ATR were expressed in *E. coli* and purified. The degree of purification was estimated to be 95% after the first step and ~99% after the final step. The specific activity and kinetic parameters for wild-type and p.I96T ATR were measured in parallel (Table 2), and similar results were obtained with and without the last hydroxyapatite purification step. The p.I96T mutant exhibits a slight reduction in specific activity, retaining 60% of wild-type levels with no significant differences in the K_ds for ATP or cobalamins, with the exception of CNCbl, which showed a 1.7-fold increase in K_d.

The oligomeric profile of the p.I96T mutant protein was analyzed by size-exclusion chromatography following ammonium sulphate precipitation and anion-exchange chromatography. Under these conditions, the protein exists mainly as a trimeric, similar to wild-type ATR (data not shown). Electrophoresis under nondenaturing conditions detected aggregates of ATR in the crude cell lysates (supernatants or pellets) with either wild-type or mutant ATR, although the size distributions were different (Fig. 4). Wild-type ATR showed lower molecular weight aggregates (~250 kDa), while the majority of the protein was present in a trimeric form. The p.I96T mutant showed both trimeric and monomeric forms. Both supernatant and crude extracts of mutant proteins showed a significant reduction in the amount of protein recovered, more pronounced in the case of p.R191W that could not be detected under any conditions (Fig. 4).

Next, we investigated the relative stabilities of the p.I96T and p.R191W mutants expressed in bacteria grown at 37°C or 27°C (Fig. 5). The p.I96T mutant was found to have a significantly decreased half life (Fig. 5A) compared to wild-type protein at 37°C (34 vs. 85 hr). At lower temperature (27°C) the half-lives for both proteins increased (Fig. 5B).

R191 projects into the central cavity of the trimeric ATR structure (Fig. 3A); interactions between this residue from adjacent monomers might play a role in stabilizing the quaternary structure of the protein. In fact, the p.R191W mutant was highly unstable at 37°C (Fig. 5A) with a half-life of 1.3 hr. The expression level of the mutant increased when the cells were grown at 27°C, with a corresponding increase in its half-life to 26.5 hr (Fig. 5B).

Wild-type and mutant ATRs were also expressed as fusion proteins with a FLAG tag in a *cblB* fibroblast cell line (P4). Cells were cultured at 37 and 27°C, and the [^{14}C]-propionate incorporation levels were determined as an indirect measure of ATR activity in the transfected cells. At 37°C, the mutant p.I96T and p.R191W proteins showed a statistically significant reduction in [^{14}C]-propionate incorporation: 65 and 52% of wild-type levels, respectively. When the cells were grown at 27°C, [^{14}C]-propionate incorporation levels of p.I96T and p.R191W mutants increased to levels close to wild-type ones (Fig. 6).

Discussion

The focus of this work was the functional analysis of five *cblB* mutations and the investigation of the underlying molecular mechanism of in vitro B_{12} responsiveness observed in three MMA patients belonging to the *cbl*B class. The results obtained indicate that all five nucleotide changes are disease-causing mutations, opening the possibility for genetic counseling, carrier identification, and prenatal diagnosis in at-risk families, and allowing determination of possible phenotype–genotype correlations and mutation-specific therapies.

Regarding the functional analysis of the exonic and intronic nucleotide changes affecting splicing, our results suggest that there are negligible levels of normal transcript associated with the mutations studied, from fibroblasts from patients and in cell lines (Hep3B, Hek293, and COS cells) transfected with the corresponding minigenes. Based on our data, the in vitro responsiveness in these patients might be associated with the missense changes, p.I96T or p.R191W. In relation to patient P4, who bears two splicing mutations, no stimulation of [^{14}C]-propionate was observed when cells were supplemented with OHCbl. However, given that the patient is clinically asymptomatic, the in-frame deletion of two amino acids resulting from the c.349−1G>C allele might a retain certain degree of activity. Addressing this will be the aim of future investigations.

The three in vitro B_{12} responsive patients (P1, P2, and P3) share the missense mutation p.I96T, which was expressed in a prokaryotic system in order to analyze its structural and kinetic properties. The mutant protein showed a modest reduction in specific activity but normal binding affinity for ATP and cob(II)alamin substrates. Inconsistent results were obtained in

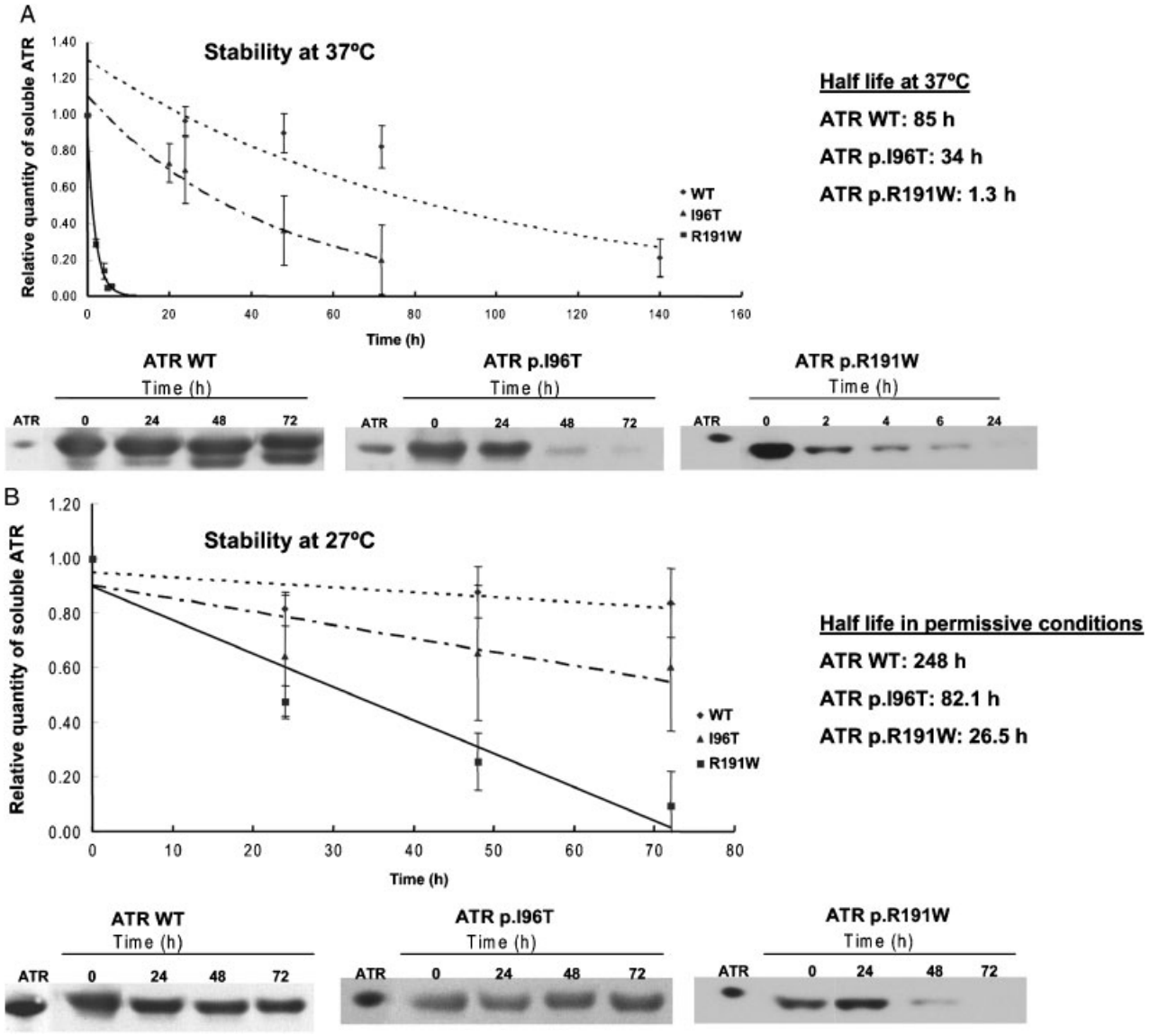

Figure 5. Degradation time course for wild-type p.I96T and p.R191W ATR at 37°C and 27°C. Crude cell extracts from cultures expressing wild-type or p.I96T or p.R191W ATR were incubated at 37°C (**A**) or 27°C (**B**) and aliquots were removed at different time points at 37 and 27°C, respectively, and subjected to SDS-PAGE and Western blot analysis as described in the Methods section. Protein amounts were quantified by laser densitometry. The data are the mean ± SD and represent the percent density of each protein relative to its density at time 0. The half-life of each protein is noted.

evaluating the effect of the mutations on the oligomeric structure of the protein. Thus, size-exclusion chromatography revealed a normal oligomeric profile, while native gel electrophoresis indicated an aberrant profile. In the former case, the purification of ATR prior to Superdex chromatography might have led to the separation of monomers, whereas the soluble or crude extracts loaded on the native gel allowed detection of all the ATR forms and involved only minor manipulation. However, the significantly lower levels of mutant protein observed by native gel electrophoresis, and the lower stability suggests that loss of biological function in the p196T mutant might be due to abnormal folding rather than a change in oligomeric state. Impaired protein folding can enhance degradation (e.g., in Gaucher and lysosomal storage disorders), lead to deposition of misfolded protein (e.g., in Alzheimer's disease) or result in an inactive form [Gamez et al., 2000; Majtan et al., 2010].

When both mutant proteins are expressed in *E. coli* under permissive low-temperature conditions, the steady-state levels of ATR and its half-life are increased. Similar results were obtained using a eukaryotic expression system where the level of ^{14}C-propionate incorporation was similar to control values when the transfected cells were grown at 27°C. Expression studies of the p.R191W mutation in *E. coli* have been previously described using a GST fusion protein in which its stability was not mentioned [Zhang et al., 2006]. In contrast, in *Salmonella enterica,* the p.R191W mutant was expressed at lower levels than the control, indicating that it impairs proper folding and leads to degradation mediated by cellular proteases [Fan and Bobik, 2008]. The residual activity associated with the pR191W mutant was reported to be 30% in the *E. coli* system and undetectable in *S. enterica* [Fan and Bobik, 2008; Zhang et al., 2006]. Mutations affecting residues close to the 191 position, for example, R190H and p.E193K, are also

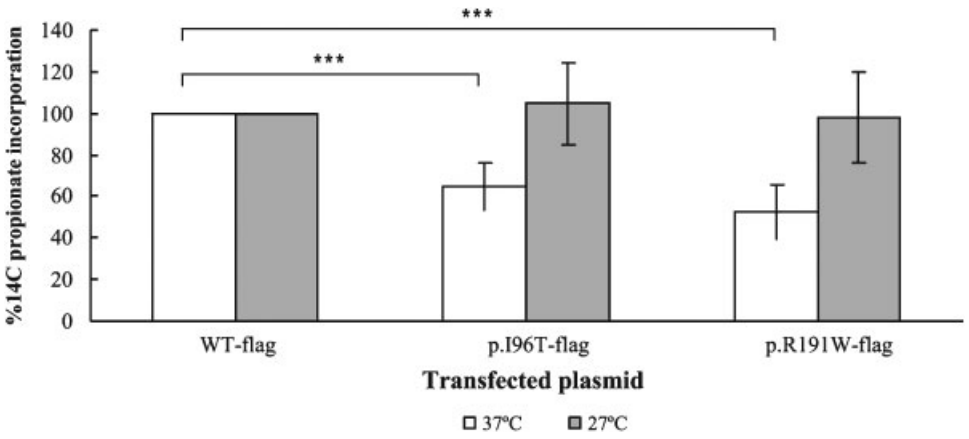

Figure 6. Functional analysis of the p.I96T and p.R191W mutants in a *cblB* null fibroblast cell line. A fibroblast cell line was transfected with a vector encoding wild-type or mutant (p.I96T or p.R191W) *MMAB* cDNA and the culture was incubated at 37 or 27°C. The cells were harvested followed by incorporation of [^{14}C]-propionate into trichloroacetic acid-precipitable material in the absence of OHCbl that was quantified as an indirect measure of ATR activity. The data are the mean ± SD of the percentage of [^{14}C]-propionate incorporation for each transfection versus the wild-type transfection ($n = 4$). The *P*-values were calculated for the pairs indicated in the figure (***P-value < 0.001).

unstable in all expression systems [Fan and Bobik, 2008; Zhang et al., 2006] and might represent a region critical for stability.

Our data suggest that p.R191W and p.196T mutants result in severe folding problems, although when expressed as fusion proteins with the Flag peptide in an eukaryotic expression system, residual activity was observed. However, because transient expression was performed using the P4 cell line, it is possible that in addition to FLAG stabilization, complementation with the endogenous ATR might have contributed to the rather high residual activity of these mutants.

The responsiveness to in vitro OHCbl supplementation could be explained partially by a stabilizing effect of the cofactor, which could act as a natural chaperone, as has been described for other cofactors, for example, tetrahydrobiopterin in phenylalanine hydroxylase deficiency [Erlandsen et al., 2004; Perez et al., 2005; Pey et al., 2004]. Other mechanisms may also be operating in the OHCbl-responsive cell line, P1, because the p.R191W mutant (albeit with a GST tag) exhibits a 16-fold higher K_M for cobalamin [Zhang et al., 2006]. Defects in ATR might also affect its interaction with MMAA or MUT proteins, assuming that the three enzymes operate in a complex and increased levels of B_{12} might have an stabilizing effect [Banerjee, 2006; Banerjee et al., 2009].

In addition to the genetic diagnosis of the disease, knowledge of the mutational spectrum in each population provides insights into genotype–phenotype correlations. Based on the clinical outcome, patients bearing the p.I96T mutation exhibit a highly variable phenotype. Thus, although one of them is clinically asymptomatic, the other two are either dead or severely neurologically impaired. These findings also suggest that the missense changes, p.I96T and p.R191W, might be categorized as a loss-of-function folding mutations that are usually associated with variable genotype–phenotype correlation [Andresen et al., 1997; Pey et al., 2003, 2007]. Interindividual differences in gene expression of the protein quality control and proteasomal proteins have been described as phenotypic modifiers in several misfolding diseases [Dipple and McCabe, 2000a,b].

In conclusion, functional analysis of the mutations described in this study is relevant to our understanding of the pathogenic mechanisms of MMA and also for the design of mutation-specific therapies. In several genetic disorders such as phenylketonuria or Gaucher's disease [Bernier et al., 2004; Mu et al., 2008; Pey et al., 2008], pharmacological rescue of folding mutants or upregulation of gene expression for mutants with residual activity is currently envisaged as a possible option for correcting, at least partially, the phenotype. In the case of the p.I96T and p.R191W mutant proteins, pharmacological chaperones or compounds such as statins [Murphy et al., 2007], which may result in activation of *MMAB* gene expression, should be explored as potential strategies to treat the disease if increased steady-state levels and activity of the protein can be achieved.

Acknowledgments

Ana Jorge-Finnigan is funded by Fondo de Investigaciones Sanitarias. This work was supported by grants from *Comisión Interministerial de Ciencia y Tecnología* (SAF2007-61350), *Fondo de Investigaciones Sanitarias* (PI060512), Fundación Ramón Areces, and the National Institutes of Health (DK45776). An institutional grant from the *Fundación Ramón Areces* to the Centro de Biología Molecular Severo Ochoa is gratefully acknowledged. We acknowledge the generous allocation of computer time at the Barcelona Supercomputing Center.

References

Andresen BS, Bross P, Udvari S, Kirk J, Gray G, Kmoch S, Chamoles N, Knudsen I, Winter V, Wilcken B, Yokota I. 1997. The molecular basis of medium-chain acyl-CoA dehydrogenase (MCAD) deficiency in compound heterozygous patients: is there correlation between genotype and phenotype? Hum Mol Genet 6:695–707.

Banerjee R. 2006. B12 trafficking in mammals: A for coenzyme escort service. ACS Chem Biol 1:149–159.

Banerjee R, Gherasim C, Padovani D. 2009. The tinker, tailor, soldier in intracellular B12 trafficking. Curr Opin Chem Biol 13:477–484.

Bernier V, Lagace M, Bichet DG, Bouvier M. 2004. Pharmacological chaperones: potential treatment for conformational diseases. Trends Endocrinol Metab 15: 222–228.

Chowdhury S, Banerjee R. 1999. Role of the dimethylbenzimidazole tail in the reaction catalyzed by coenzyme B12-dependent methylmalonyl-CoA mutase. Biochemistry 38:15287–15294.

Case TAD, CheathamIII TE, Simmerling CL, Wang J, Duke RE, Luo R, Crowley M, Walker RC, Zhang W, Merz KM, Wang B, Hayik S, Roitberg A, Seabra G, Kolossváry I, Wong KF, Paesani F, Vanicek J, Wu X, Brozell SR, Steinbrecher T, Gohlke H, Yang L, Tan C, Mongan J, Hornak V, Cui G, Mathews DH, Seetin MG, Sagui C, Babin V, Kollman PA. 2008. AMBER 10. San Francisco: University of California.

DeLano WL. 1998–2003. The PyMOL Molecular Graphics System. Version 0.93. San Carlos, CA: DeLano Scientific LLC.

Dipple KM, McCabe ER. 2000a. Modifier genes convert "simple" Mendelian disorders to complex traits. Mol Genet Metab 71:43–50.

Dipple KM, McCabe ER. 2000b. Phenotypes of patients with "simple" Mendelian disorders are complex traits: thresholds, modifiers, and systems dynamics. Am J Hum Genet 66:1729–1735.

Dobson CM, Wai T, Leclerc D, Kadir H, Narang M, Lerner-Ellis JP, Hudson TJ, Rosenblatt DS, Gravel RA. 2002. Identification of the gene responsible for the cblB complementation group of vitamin B12-dependent methylmalonic aciduria. Hum Mol Genet 11:3361–3369.

Duan Y, Wu C, Chowdhury S, Lee MC, Xiong G, Zhang W, Yang R, Cieplak P, Luo R, Lee T, Caldwell J, Wang J, Kollman P. 2003. A point-charge force field for molecular mechanics simulations of proteins based on condensed-phase quantum mechanical calculations. J Comput Chem 24: 1999–2012.

Erlandsen H, Pey AL, Gamez A, Perez B, Desviat LR, Aguado C, Koch R, Surendran S, Tyring S, Matalon R, Scriver CR, Ugarte M, Martínez A, Stevens RC. 2004. Correction of kinetic and stability defects by tetrahydrobiopterin in phenylketonuria patients with certain phenylalanine hydroxylase mutations. Proc Natl Acad Sci USA 101:16903–16908.

Eswar N, Webb B, Marti-Renom MA, Madhusudhan MS, Eramian D, Shen MY, Pieper U, Sali A. 2006. Comparative protein structure modeling using Modeller. Curr Protoc Bioinformatics Chapter 5:Unit 56.

Fan C, Bobik TA. 2008. Functional characterization and mutation analysis of human ATP:Cob(I)alamin adenosyltransferase. Biochemistry 47:2806–2813.

Gamez A, Perez B, Ugarte M, Desviat LR. 2000. Expression analysis of phenylketonuria mutations: effect on folding and stability of the phenylalanine hydroxylase protein. J Biol Chem 275:29737–29742.

Gentleman R. 1997. R. Version 2.9.2. Vienna: R Foundation for Statistical Computing. http://www.R-project.org.

Gordon JC, Myers JB, Folta T, Shoja V, Heath LS, Onufriev A. 2005. H++: a server for estimating pKas and adding missing hydrogens to macromolecules. Nucleic Acids Res 33:W368–W371.

Johnson CL, Pechonick E, Park SD, Havemann GD, Leal NA, Bobik TA. 2001. Functional genomic, biochemical, and genetic characterization of the Salmonella pduO gene, an ATP:cob(I)alamin adenosyltransferase gene. J Bacteriol 183: 1577–1584.

Leal NA, Olteanu H, Banerjee R, Bobik TA. 2004. Human ATP:Cob(I)alamin adenosyltransferase and its interaction with methionine synthase reductase. J Biol Chem 279:47536–47542.

Leal NA, Park SD, Kima PE, Bobik TA. 2003. Identification of the human and bovine ATP:Cob(I)alamin adenosyltransferase cDNAs based on complementation of a bacterial mutant. J Biol Chem 278:9227–9234.

Majtan T, Liu L, Carpenter JF, Kraus JP. 2010. Rescue of cystathionine beta-synthase (CBS) mutants with chemical chaperones: purification and characterization of eight CBS mutant enzymes. J Biol Chem 285:15866–15873.

Martinez MA, Rincon A, Desviat LR, Merinero B, Ugarte M, Perez B. 2005. Genetic analysis of three genes causing isolated methylmalonic acidemia: identification of 21 novel allelic variants. Mol Genet Metab 84:317–325.

Merinero B, Perez B, Perez-Cerda C, Rincon A, Desviat LR, Martinez MA, Sala PR, Garcia MJ, Aldamiz-Echevarria L, Campos J, Cornejo V, Del Toro M, Mahfoud A, Martínez-Pardo M, Parini R, Pedrón C, Peña-Quintana L, Pérez M, Pourfarzam M, Ugarte M. 2008. Methylmalonic acidaemia: examination of genotype and biochemical data in 32 patients belonging to mut, cblA or cblB complementation group. J Inherit Metab Dis 31:55–66.

Mu TW, Ong DS, Wang YJ, Balch WE, Yates 3rd JR, Segatori L, Kelly JW. 2008. Chemical and biological approaches synergize to ameliorate protein-folding diseases. Cell 134:769–781.

Murphy C, Murray AM, Meaney S, Gafvels M. 2007. Regulation by SREBP-2 defines a potential link between isoprenoid and adenosylcobalamin metabolism. Biochem Biophys Res Commun 355:359–364.

Ortiz AR, Strauss CE, Olmea O. 2002. MAMMOTH (matching molecular models obtained from theory): an automated method for model comparison. Protein Sci 11:2606–2621.

Pavlidis P, Noble WS. 2003. Matrix2png: a utility for visualizing matrix data. Bioinformatics 19:295.

Perez B, Desviat LR, Gomez-Puertas P, Martinez A, Stevens RC, Ugarte M. 2005. Kinetic and stability analysis of PKU mutations identified in BH4-responsive patients. Mol Genet Metab 86:S11–S16.

Perez-Cerda C, Merinero B, Sanz P, Jimenez A, Garcia MJ, Urbon A, Diaz Recasens J, Ramos C, Ayuso C, Ugarte M. 1989. Successful first trimester diagnosis in a pregnancy at risk for propionic acidaemia. J Inherit Metab Dis 12:274–276.

Pey AL, Desviat LR, Gamez A, Ugarte M, Perez B. 2003. Phenylketonuria: genotype–phenotype correlations based on expression analysis of structural and functional mutations in PAH. Hum Mutat 21:370–378.

Pey AL, Perez B, Desviat LR, Martinez MA, Aguado C, Erlandsen H, Gamez A, Stevens RC, Thorolfsson M, Ugarte M, Martínez A. 2004. Mechanisms underlying responsiveness to tetrahydrobiopterin in mild phenylketonuria mutations. Hum Mutat 24:388–399.

Pey AL, Stricher F, Serrano L, Martinez A. 2007. Predicted effects of missense mutations on native-state stability account for phenotypic outcome in phenylketonuria, a paradigm of misfolding diseases. Am J Hum Genet 81:1006–1024.

Pey AL, Ying M, Cremades N, Velazquez-Campoy A, Scherer T, Thony B, Sancho J, Martinez A. 2008. Identification of pharmacological chaperones as potential therapeutic agents to treat phenylketonuria. J Clin Invest 118:2858–2867.

Rincon A, Aguado C, Desviat LR, Sanchez-Alcudia R, Ugarte M, Perez B. 2007. Propionic and methylmalonic acidemia: antisense therapeutics for intronic variations causing aberrantly spliced messenger RNA. Am J Hum Genet 81:1262–1270.

Saridakis V, Yakunin A, Xu X, Anandakumar P, Pennycooke M, Gu J, Cheung F, Lew JM, Sanishvili R, Joachimiak A, Arrowsmith CH, Christendat D, Edwards AM. 2004. The structural basis for methylmalonic aciduria. The crystal structure of archaeal ATP:cobalamin adenosyltransferase. J Biol Chem 279:23646–23653.

Schubert HL, Hill CP. 2006. Structure of ATP-bound human ATP:cobalamin adenosyltransferase. Biochemistry 45:15188–15196.

St. Maurice M, Mera PE, Taranto MP, Sesma F, Escalante-Semerena JC, Rayment I. 2007. Structural characterization of the active site of the PduO-type ATP:Co(I)rrinoid adenosyltransferase from *Lactobacillus reuteri*. J Biol Chem 282:2596–2605.

Still WC, Tempczyk A, Hawley RC, Hendrickson T. 2002. Semianalytical treatment of solvation for molecular mechanics and dynamics. J Am Chem Soc 112:6127–6129.

Weiser J, Shenkin PS, Still WC. 1999. Approximate atomic surfaces from linear combinations of pairwise overlaps (LCPO). J Comput Chem 20:217–230.

William LJ, Jayaraman C, Jeffry DM, Roger WI, Michael LK. 1983. Comparison of simple potential functions for simulating liquid water. J Chem Phys 79:926–935.

Yamanishi M, Labunska T, Banerjee R. 2005. Mirror "base-off" conformation of coenzyme B12 in human adenosyltransferase and its downstream target, methylmalonyl-CoA mutase. J Am Chem Soc 127:526–527.

Zhang J, Dobson CM, Wu X, Lerner-Ellis J, Rosenblatt DS, Gravel RA. 2006. Impact of cblB mutations on the function of ATP:cob(I)alamin adenosyltransferase in disorders of vitamin B12 metabolism. Mol Genet Metab 87: 315–322.